scientific reports

Check for updates

OPEN

Investigation of electrochromic performances of multicolor V_2O_5 devices fabricated at low processing temperature

Ming-Yue Tan[1], Gregory Soon How Thien[1], Kar-Ban Tan[2], H. C. Ananda Murthy[3,4] & Kah-Yoong Chan[1]✉

In recent decades, poorly insulated windows have increased the energy consumption of heating and cooling systems, thus contributing to excessive carbon dioxide emissions and other related pollution issues. From this perspective, the electrochromic (EC) windows could be a tangible solution as the indoor conditions are highly controllable by these smart devices even at a low applied voltage. Literally, vanadium pentoxide (V_2O_5) is a renowned candidate for the EC application due to its multicolor appearance and substantial lithium insertion capacity. Despite the growing interest in V_2O_5 thin films, only limited literature study is available for V_2O_5 films specifically the annealing effects of these films at lower temperatures (< 300 °C). It is noteworthy that a low temperature is advantageous for glass-based EC devices, as it prevents deformation, cracking, and structural damage to the transparent conductive glass. In this study, V_2O_5 thin films were fabricated using the sol–gel spin coating technique prior to annealing over the temperature range of 100–300 °C. Subsequently, V_2O_5 thin films were assembled into a device form to analyze their EC characteristics. The V_2O_5 device, featuring thin film annealed at 200 °C, demonstrated excellent EC performance with high optical contrast of 42.32%, high coloration efficiency (CE) of 34.93 cm^2/C, as well as rapid coloring and bleaching times of 0.4 s and 3 s, respectively. These results shed light on the importance of annealing temperature control towards the EC performance of V_2O_5 devices for future applications.

Keywords Electrochromic, Vanadium pentoxide, Annealing temperature, Sol–gel spin-coating

Over the past few decades, the world has experienced unprecedented challenges related to the depletion of energy and other environmental issues. The preponderance of evidence[1,2] also indicated that global warming is mainly due to human activities, particularly the emissions of heat-trapping greenhouse gases. As such, the electrochromic (EC) windows could be an alternative due to their capability to regulate the ambient conditions within indoor spaces by utilizing a low voltage. In other words, this serves to reduce the energy consumption of heating and cooling systems and to prevent the excessive emission of carbon dioxide[3]. Moreover, EC smart windows offer multiple advantages over traditional windows for residential and commercial building premises, including improved comfort as well as enhanced visual and thermal satisfaction for occupants. Additionally, these windows are also widely adopted in both the automotive and construction industries[4,5].

Electrochromism, the phenomenon where materials change color in response to an electrical stimulus, finds its roots in the discovery of Prussian blue (also known as hexacyanoferrate) in 1704 by Diesbach[6]. The color change of this compound from transparent to blue was due to the oxidized iron. On the other hand, the first demonstration of electrochromic coloration using WO_3 thin films was shown in 1969[7] and this was followed by tremendous research in EC technology, wherein significant breakthroughs and technological advancements were discovered over time. Literally, EC devices consist of metal oxide thin films and electrolytes sandwiched between two transparent conductive electrodes[8]. Tungsten trioxide (WO_3)[9], vanadium oxide (VOx)[10], titanium

[1]Centre for Advanced Devices and Systems, Faculty of Engineering, Multimedia University, Persiaran Multimedia, 63100 Cyberjaya, Selangor, Malaysia. [2]Department of Chemistry, Faculty of Science, Universiti Putra Malaysia, 43400 Serdang, Selangor, Malaysia. [3]Department of Applied Sciences, Papua New Guinea University of Technology, Lae, Morobe Province 411, Papua New Guinea. [4]Department of Prosthodontics, Saveetha Dental College and Hospital, Saveetha Institute of Medical and Technical Science (SIMATS), Saveetha University, Chennai, Tamil Nadu 600077, India. ✉email: kychan@mmu.edu.my

dioxide (TiO_2)[11], nickel oxide (NiO)[12], and iridium oxide (IrO_2)[13] are some of the notable metal oxides utilized in the EC device applications. Among these EC materials, WO_3 has been widely recognized for its superior coloration efficiency and excellent cyclic stability[14]. Nevertheless, the application of WO_3 has been hindered by its ability to display only monotonous color (dark blue) during coloration[15]. This monochromatic feature not only restricts its functionality in the EC windows but also limits its practical application in display technologies due to the full-color requirement of modern electronic devices for graphics, text, and video. Additionally, this limitation could potentially reduce its marketability, as consumers tend to favor devices with multicolor options.

These days, vanadium oxide (Vox) is a promising candidate for the development of multicolor EC devices owing to its substantial lithium insertion capacity and varying oxidation states (V^{2+} to V^{5+})[16]. V_2O_5 has been in the most stable form due to its fully oxidized phase (+5) and stable electron configuration[17,18]. To further elaborate, V_2O_5 is structured around distorted VO_6 octahedra, wherein each vanadium cation is centrally coordinated by six oxygen anions. These octahedra share edges and corners, thereby forming a continuous network within the layers. Furthermore, the adjacent layers are bound by van der Waals forces, which results in the formation of a three-dimensional framework[19]. The versatility and distinctive chemical properties of V_2O_5 play a crucial role in various applications. For instance, V_2O_5 films function as hole transport layers in solar cells[20], find utility in conductometric gas sensors[21], act as humidity sensors[22], and serve as a gate dielectric in MOSFETs[23]. Meanwhile, V_2O_5 thin films with multicolor features can be integrated into energy storage devices whose energy status is indicated through optical contrast[24]. These films are also used in color-switchable EC windows with enhanced functionality and aesthetics. Notably, V_2O_5 exhibits both cathodic and anodic coloration electrochromism, thus allowing it to function effectively either as a color-changing layer or an ion storage layer within an EC device[16,25]. Previous researchers have utilized a range of methods such as sol–gel spin coating[26], spray pyrolysis deposition[27], hydrothermal synthesis[28], and chemical vapor deposition[29] for the deposition of V_2O_5 thin films. Among these methods, the sol–gel process is notable for its simplicity, uniform coating, submicron thickness, and cost-effectiveness for the deposition of a variety of EC films[14,30,31].

The varying factors such as fabrication technique, deposition method, and annealing conditions can affect the chemical stoichiometry, phase purity, and crystallinity of the prepared V_2O_5 films. For instance, the V_2O_5 thin films synthesized via spray pyrolysis and annealed over a temperature range of 300–500 °C were found to be a mixture of orthorhombic α-V_2O_5 phases, along with minor quantities of β-V_2O_5 and tetragonal V_4O_9 phases[27]. In a related work, the effect of annealing on the structural properties of V_2O_5 thin films by direct current (DC) magnetron sputtering was studied[32]. Prior to annealing, the XRD analysis showed no discernible peaks, confirming the amorphous nature of these thin films. On the contrary, a prominent peak emerged along the V_2O_5 (010) direction after annealing at 480 °C, demonstrating improved film crystallinity. These studies also suggested that low annealing temperature is noteworthy for further research specifically a lower temperature range is beneficial for glass-based EC devices, as it prevents deformation, cracking, thermal stress, and structural damage to the transparent conductive glass[33,34]. In addition, the development of flexible EC devices requires a low annealing temperature to avoid damage to their plastic substrates[35].

Hence, in this study, V_2O_5 thin films were deposited using the sol–gel spin coating technique, followed by annealing at temperatures ranging from 100 to 300 °C. Subsequently, V_2O_5 thin films were assembled into a device form, and their optical, structural, and EC characteristics were analyzed. This study highlighted the potential of V_2O_5 devices for future electronic applications including the creation of multicolor windows for lifestyle and the development of versatile multicolor displays[36].

Materials and methods

All chemicals utilized in the present work were of analytical grade and were purchased from Sigma-Aldrich, Rockville, MD, USA. Additionally, indium tin oxide (ITO) glass substrates with a sheet resistance of 15 Ω/sq were purchased from Han Xin Industry Co., Ltd., Shanghai, China. The main ingredients used in the V_2O_5 sol–gel synthesis included V_2O_5 powder, hydrogen peroxide (H_2O_2), and distilled water.

The V_2O_5 sol–gel process was initiated by dissolved V_2O_5 powder with H_2O_2 solution (15%) in a conical flask. The mixture was then heated to 70 °C and stirred vigorously, resulting in a yellow–orange solution. After several minutes, the solution underwent an exothermic reaction, transforming into a viscous dark red solution. Before the deposition of V_2O_5 sol–gel, the ITO glass substrates were subjected to a thorough cleaning process involving ultrasonic baths with soap, ethanol, acetone, and distilled water.

The V_2O_5 sol–gel was deposited onto the ITO glass substrates using the spin coating technique, with a rotation speed of 1500 rpm for 30 s. Following this, the fresh V_2O_5 layer was dried on a hot plate for 3 min to remove extra solvent and prevent potential surface scratches. These steps were repeated multiple times to achieve the desired thickness. Subsequently, the samples, each with an active area of 2.4 cm^2, were annealed at temperatures ranging from 100 to 300 °C for 1 h. Lastly, V_2O_5 devices were assembled in the following order: ITO/V_2O_5 thin film/Li^+ gel electrolyte/ITO and were sealed using UV resin [see Fig. 1]. Notably, the Li^+ gel electrolyte was prepared using lithium perchlorate ($LiClO_4$), polycarbonate (PC) and polymethyl methacrylate (PMMA) as the primary ingredients, as adapted from our previous work[37]. The addition of PMMA to the electrolyte helps to modulate its viscosity, ensuring ease of handling during device assembly and preventing electrolyte leakage. Moreover, PMMA offers excellent light transmission and high ionic conductivity when combined with synthetic Li^+ salts, thus contributing to the overall stability of EC devices[38].

The physical properties of the V_2O_5 thin films were characterized using an X-ray diffractometer (XRD, Shimadzu) with Cu Kα radiation (λ = 1.5406 Å) over the 2θ range of 10 to 70°. Besides, field emission scanning electron microscopy (FESEM, Nova NanoSEM 450) was employed to study both the surface morphology and cross-sectional region of the prepared films. Similarly, atomic force microscopy (AFM, Nanosurf Easyscan 2) was utilized to measure the surface roughness and topographical features of the thin films. Meanwhile, energy-dispersive X-ray (EDX, Oxford Instruments) spectroscopy was used for the elemental analysis. Furthermore, the

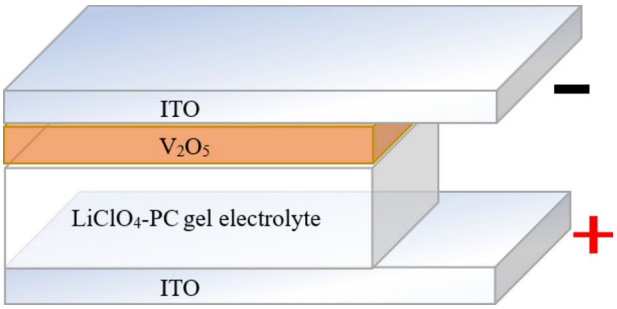

Fig. 1. V_2O_5 device structure.

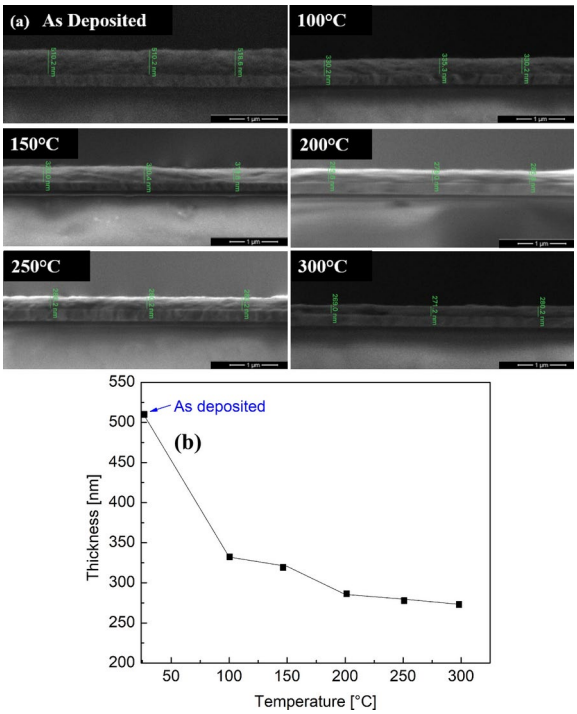

Fig. 2. (**a**) Thickness variations across different positions and (**b**) average thickness of V_2O_5 thin films at different annealing temperatures.

optical transmittances of the V_2O_5 devices were studied using an ultraviolet–visible (UV–Vis, Avantes AvaSpec-2048L) spectrophotometer. Lastly, chronoamperometry (CA) and cyclic voltammetry (CV) analyses (Autolab PGSTAT204) were utilized for the investigation of the EC characteristics. A two-electrode electrochemical setup was employed with V_2O_5 thin film as the working and reference electrode, and ITO served as the counter electrode.

Results and discussion

Structural properties of V_2O_5 thin films

Figure 2a illustrates the thickness variation of the V_2O_5 thin films across different positions, while Fig. 2b presents the average thickness of thin films annealed at temperatures between 100 and 300 °C, as determined by FESEM measurements. The as-deposited V_2O_5 films demonstrated a maximum average thickness of 513 nm but were found to decrease significantly after the annealing process. Specifically, V_2O_5 thin films annealed at 100, 150, 200, 250, and 300 °C exhibited a gradual decrease in their average thickness with the respective values of 332, 320, 284, 280, and 273 nm. Notably, increasing the annealing temperature could enhance the molecular activity within these thin films, wherein their bonding with the substrate was weakened due to the thermal disruption[39]. Consequently, these films displayed greater compactness and reduced overall thickness[39].

Figure 3 illustrates the XRD patterns of V_2O_5 thin films subjected to different annealing temperatures. In general, higher annealing temperatures improved the crystallinity of the V_2O_5 thin films, as evidenced by the XRD analysis.

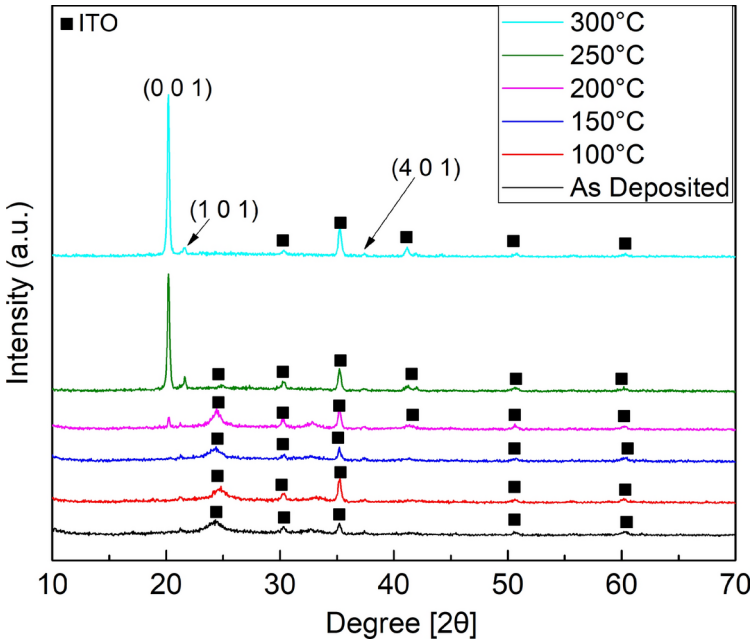

Fig. 3. XRD patterns of V_2O_5 thin films at different annealing temperatures.

The as-deposited thin film displayed two small peaks at angles of 22° and 37°, corresponding to the Miller indices (101) and (401) respectively. These peaks indicated the presence of orthorhombic structured V_2O_5 with space group Pmmn (ICDD no. 01-089-0612), suggesting that the thin film was of low crystallinity prior to annealing. Meanwhile, V_2O_5 thin films annealed at temperatures of 100, 150, and 200 °C demonstrated similar XRD planes to those of the as-deposited film. The results indicated that these films were of poor crystallinity due to the low annealing temperatures. Interestingly, at an annealing temperature of 200 °C, a V_2O_5 peak corresponding to the (001) lattice plane was discernible at an angle of 20°, thus suggesting the onset of polycrystalline growth. As the temperature was increased to 250 °C and above, the more pronounced (001) plane served to signify the enhanced crystallinity and improved structural order within these thin films. Kabir et al. suggested that a higher annealing temperature could reduce lattice defects and induce modified atomic arrangement within the thin film, ultimately improving its crystalline quality[40]. Furthermore, temperatures above 200 °C exhibited a stronger presence of (001) peaks, indicating their increased dominance at higher temperatures.

Figure 4 depicts FESEM images of V_2O_5 thin films annealed at various temperatures. The results revealed that all these thin films displayed uneven surfaces, suggesting a lack of uniformity and smoothness. Meanwhile, the as-deposited V_2O_5 thin film, as well as thin films annealed at 100 °C and 150 °C, exhibited tightly packed worm-like nanoparticles, with clear boundaries between individual particles. Upon annealing at 200 °C, the worm-like structure remained, but these particles were arranged further apart, resulting in noticeable pinholes. At annealing temperatures of 250 °C and 300 °C, the particles agglomerated to form larger clusters, causing their shape to become irregular with less distinct boundaries. Furthermore, the increased grain size at higher temperatures also caused these thin films to have a relatively coarser appearance.

Figure 5 presents the AFM morphology and topography of V_2O_5 thin films annealed at different temperatures, measured over 3 × 3 µm areas. The unannealed film displayed a root mean square (RMS) roughness of 6.0 nm. Upon annealing at 100 °C, the RMS roughness slightly increased to 6.43 nm. Further annealing at 200 °C and 300 °C resulted in RMS roughness values of 8.03 nm and 9.0 nm, respectively, attributed to the emergence of a polycrystalline structure within the film[41].

Elemental composition of V_2O_5 thin films

Table 1 tabulates the weight percentages (Wt%) of the elements in V_2O_5 thin films annealed at different temperatures, as extracted from the EDX analysis. Given that these films were deposited on ITO glass substrates, the presence of indium and tin elements was also detected. The results indicated the absence of impurity elements other than vanadium (V), oxygen (O), indium (In), and tin (Sn). Furthermore, the V percentage reduced gradually from 42.1 to 35% at 250 °C before a sharp increment to 55.6% at 300 °C. Notably, with an EDX penetration depth of 1 µm and a V_2O_5 film thickness of approximately 300 nm, the detected oxygen content likely originated not only from the V_2O_5 film but also from the underlying ITO glass substrate and potentially the surrounding environment.

Optical properties of V_2O_5 thin films

The optical transmittances of V_2O_5 thin films at varying annealing temperatures are illustrated in Fig. 6a. Without annealing, the V_2O_5 thin film exhibited low transparency of 70%, primarily due to its greater thickness [see Fig. 2b], thereby resulting in reduced light transmission. On the contrary, the thin films annealed from 100

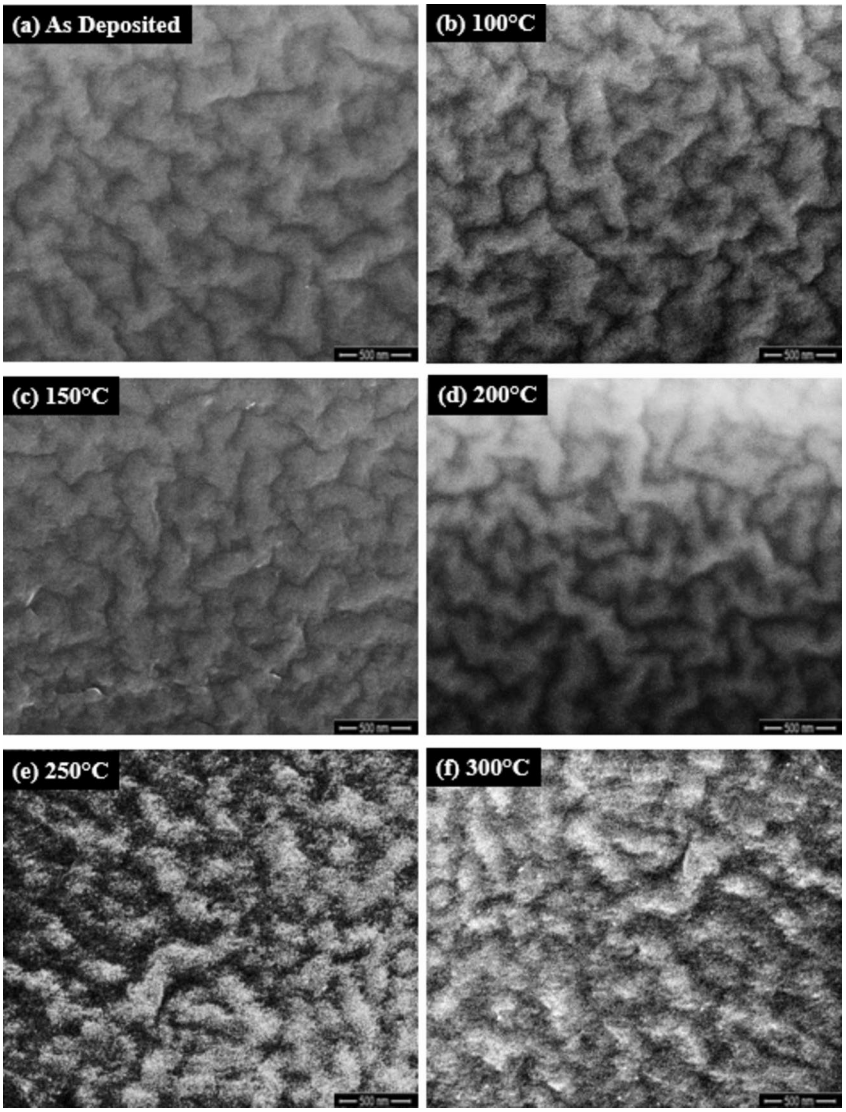

Fig. 4. FESEM images of V_2O_5 thin films annealed at (**a**) As-Deposited, (**b**) 100 °C, (**c**) 150 °C, (**d**) 200 °C, (**e**) 250 °C and (**f**) 300 °C.

to 300 °C achieved a high average film transmittance of 85%. Furthermore, the interference fringe depicted in Fig. 6a is caused by the incident light reflecting between the thin films, air, and glass substrates.

To determine the optical band gaps of the V_2O_5 thin films at various annealing temperatures, Tauc plot analysis [see Fig. 6b] is performed using the following Tauc equation[42]:

$$(\alpha h\nu)^n = \mathrm{A}(h\nu - E_g) \tag{1}$$

where α is the absorption coefficient (cm^{-1}), h is the Plank's constant (6.626×10^{-34} J.s), ν is the frequency of the incident light (Hz), n indicates the nature of the electronic transition (with $n = 2$ for direct band gap and $n = ½$ for indirect bandgap), A is the proportional constant, $h\nu$ is the incident photon energy (eV), and E_g is the band gap of the material (eV).

The observed linear region in the Tauc plot for $(\alpha h\nu)^2$ versus $h\nu$ [see Fig. 6b] indicated a direct band gap for the V_2O_5 thin films[43]. The E_g values determined by extrapolating the linear portion of the plots ranged from 2.2 to 2.5 eV and were aligned with previous studies[44–46]. The analysis demonstrated an increase in E_g from 2.2 to 2.4 eV as the annealing temperature rose from 100 to 200 °C. This was attributed to the growing grain size and reduced structural defects at higher temperatures[47]. Beyond 200 °C, E_g stabilized around 2.4 eV, indicating that further annealing had minimal effect on the electronic structure of the thin film. However, several studies reported a decrease in the band gap with higher annealing temperatures, attributed to changes in the microstructure of thin film, improved surface roughness, and an increase in oxygen vacancies that introduced free electrons and enhanced conductivity[32,42,48,49]. The discrepancy between the present study and previous findings might result from variations in thin film preparation methods and experimental conditions[32].

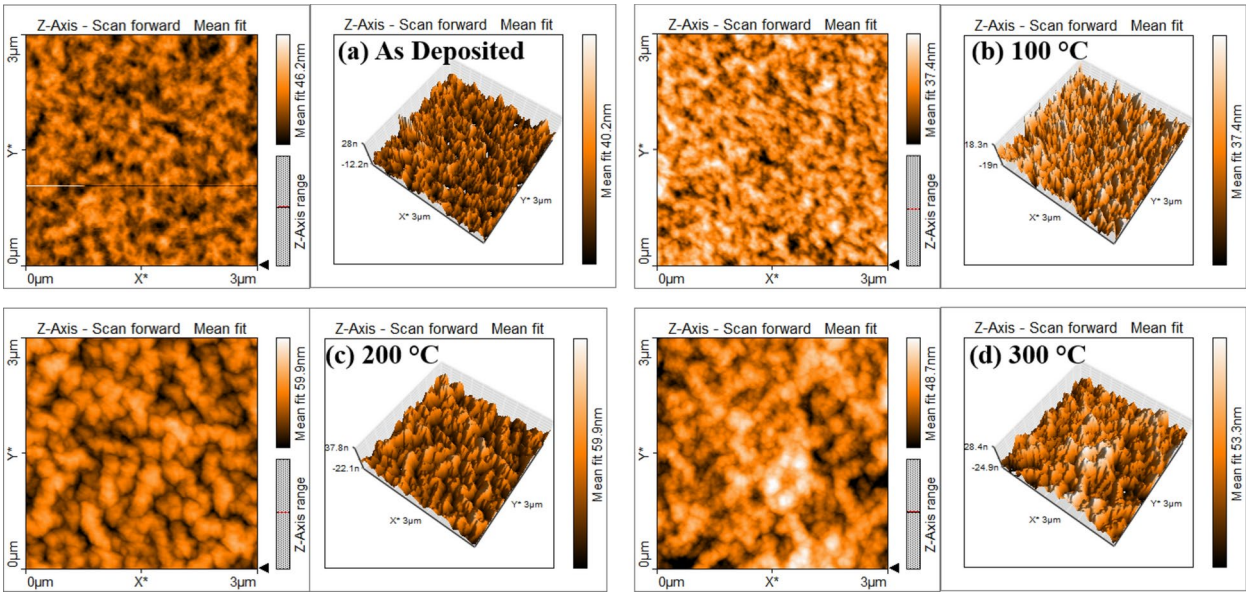

Fig. 5. AFM images of V_2O_5 thin films annealed at (**a**) As-Deposited, (**b**) 100 °C, (**c**) 200 °C, and (**d**) 300 °C.

	Wt%					
Annealing Temperature (°C)	**As Deposited**	**100**	**150**	**200**	**250**	**300**
O	12.9	12.9	14.2	19.6	17.8	9.1
V	42.1	48.7	45.1	36.5	35.0	55.6
In	38.0	37.2	37.4	42.0	47.2	32.7
Sn	7.0	1.2	3.3	1.9	0.0	2.7

Table 1. Elemental composition of V_2O_5 thin films at various annealing temperatures.

EC properties of V_2O_5 devices

Figure 7a–c present the cyclic voltammograms (CV) of V_2O_5 devices incorporating as-deposited thin films and those annealed at 200 °C and 300 °C, measured at scan rates varying from 25 to 150 mV/s. The results indicated that both anodic (I_{pa}) and cathodic peak (I_{pc}) currents demonstrated a linear relationship with the square root of the scan rate between 25 and 150 mV/s, suggesting a diffusion-controlled process[50]. Furthermore, Fig. 7d displays the 10th-cycle CV measurements for the V_2O_5 devices at different annealing temperatures, using a linear voltage sweep from − 2 to 2 V at a scan rate of 0.1 V/s. The measurements indicated that all V_2O_5 devices, except for the one annealed at 250 °C, displayed two distinct cathodic and anodic peaks in their CV curves, indicating a two-step electrochromic transition during the potential sweeps[51]. These peaks were associated with phase transitions of $Li_xV_2O_5$ during Li^+ ion insertion and extraction[51]. To further elaborate, V^{5+} ions were partially reduced to $V^{5+/4+}$ during the first reduction, thus resulting in a color change from orange to yellow–green. In the second reduction, $V^{5+/4+}$ ions were fully reduced to V^{4+}, changing the V_2O_5 devices from yellow–green to blue. Conversely, the oxidation process was the opposite of the reduction process, with the color of the V_2O_5 devices changing from blue to yellow–green and back to their original orange color [see Supplementary Fig. S1][51]. The redox process can be explained using the following equation[52]:

$$V_2O_5 + xLi^+ + xe^- \leftrightarrow Li_xV_2O_5 \quad (2)$$

where x refers to the concentration of ions.

Based on Fig. 7d, the cathodic peak current was found to increase from 1.31 mA at 100 °C to 2.24 mA at 200 °C. However, with the annealing temperature increased to 250 °C and 300 °C, the cathodic peak current decreased to 0.70 mA and 0.47 mA, respectively. This observation was attributed to the reduced defects and increased crystallinity within these V_2O_5 thin films, which consequently hindered its ability to accommodate ion penetration[53]. On the contrary, the thin films annealed at lower temperatures exhibited a less crystalline structure, which could facilitate ease of Li^+ ions diffusion during the redox process[53]. These observations were consistent with the literature[54], where the cathodic peak current reached its maximum at 60 °C and subsequently decreased at higher annealing temperatures. It is worth highlighting that the porous thin films prepared at lower annealing temperatures could offer a shortened ion diffusion pathway facilitating electrolyte penetration. Conversely, at higher annealing temperatures, reduced ion mobility in the thin films was observed due to larger grain sizes and/or a reduction in cracks.

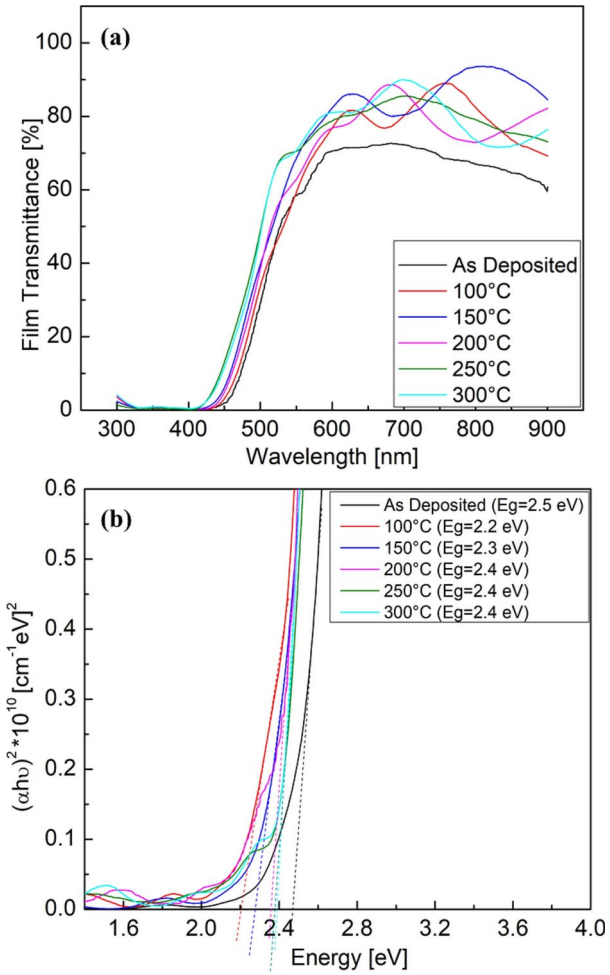

Fig. 6. (**a**) Optical transmittance spectra (**b**) optical band gaps of V_2O_5 thin films at different annealing temperatures.

Furthermore, the cathodic peak current at a scan rate of 0.1 V/s, extracted from the CV graphs [Fig. 7a–c] can be inserted into the Randles Sevcik equation to calculate the diffusion coefficient, *D*, of Li^+ ions during the redox reaction as follows[55]:

$$i_p = 2.69 \times 10^5 \times A \times n^{\frac{3}{2}} \times D^{\frac{1}{2}} \times C_o \times \upsilon^{\frac{1}{2}} \quad (3)$$

where i_p is the cathodic peak currents, *A* is the electrode surface area (2.4 cm^2), n is the number of electrons (value = 1), *D* is the diffusion coefficient, C_o is the electrolyte concentration (1 mol/L), and υ is the scan rate (0.1 V/s). Table 2 presents the diffusion coefficients of V_2O_5 devices at different post-annealing temperatures. The analysis demonstrated that V_2O_5 devices annealed at 200 °C achieved the highest diffusivity of 12.15×10^{-11} cm^2/s, suggesting an enhanced kinetic response in the EC devices[56]. However, at annealing temperature beyond 200 °C, the diffusivity was found to decrease significantly due to the blocking of insertion sites[57].

Optical modulation is a crucial parameter in evaluating the performance of EC devices, as it quantifies the degree of color change during both the coloring and bleaching states. Notably, high transmittance during the bleaching state and low opacity during the coloring state could contribute to higher optical modulation. To measure the optical contrast, V_2O_5 devices were subjected to chronoamperometry (CA) measurement with a step potential of − 2/ + 2 V. Subsequently, UV–vis spectroscopy was employed to measure the optical transmittance of the V_2O_5 devices at a wavelength of 633 nm. Figure 8 depicts the optical contrast of V_2O_5 devices at varying annealing temperatures, while Table 3 lists the coloring, bleaching, and optical transmittance values corresponding to different annealing temperatures.

Figure 8 demonstrates that V_2O_5 devices with unannealed thin film exhibited a relatively high optical modulation of 29.56%, indicating that color changes can occur without annealing. As the annealing temperature increased from 100 to 200 °C, an enhancement of the optical modulation was achieved but these values were found to decrease significantly at elevated temperatures. Specifically, V_2O_5 devices annealed at 200 °C exhibited the highest optical modulation of 42.32%, attributed to their low coloring transmittance of 29.57% and high bleaching transmittance of 71.89%. In contrast, the optical modulation at annealing temperatures of 250 °C

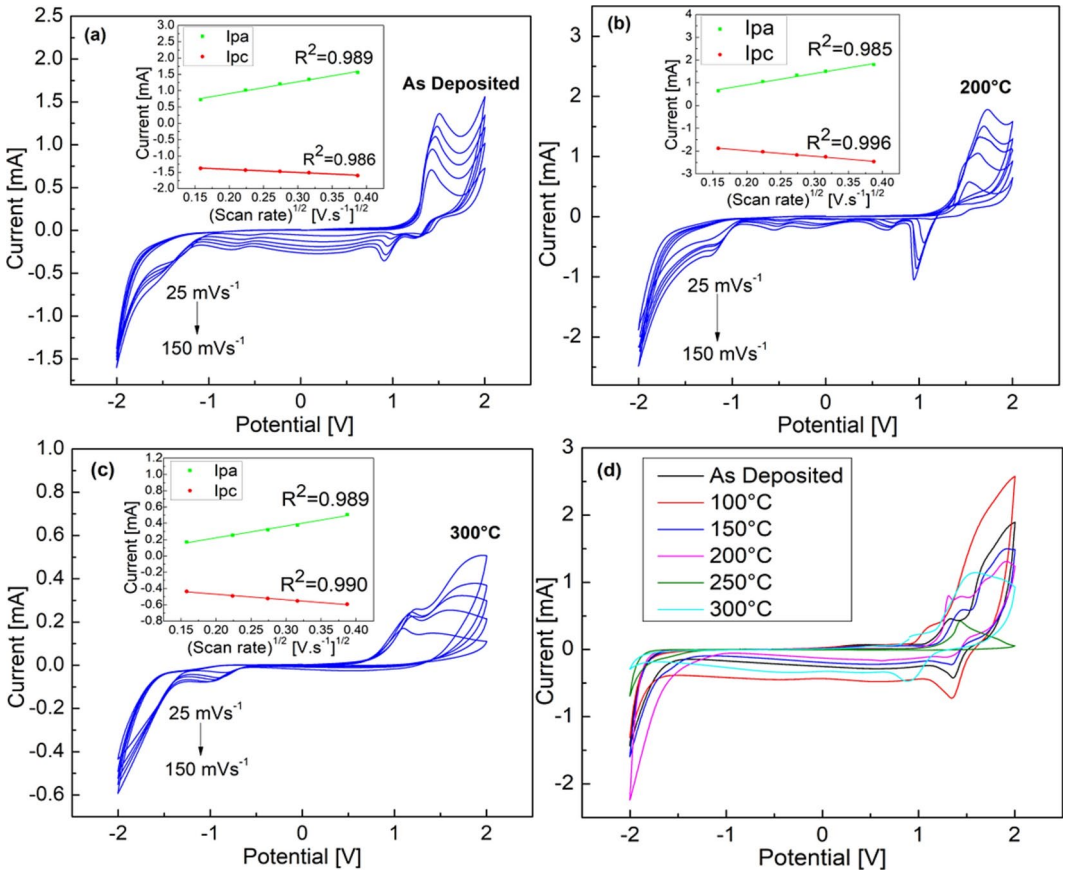

Fig. 7. Cyclic voltammograms of V_2O_5 devices: (**a**–**c**) CV curves for as-deposited and annealed films (200 °C and 300 °C) at scan rates of 25–150 mV/s; (**d**) 10th-cycle CV curves at different annealing temperatures with a sweep from -2 to 2 V at 0.1 V/s.

Temperature (°C)	Cathodic Peak Current, I_{pc} (mA)	Cathodic Diffusion Coefficient, D_c (10^{-11} cm^2 s^{-1})
As Deposited	− 1.50	4.46
200	− 2.25	12.15
300	− 0.55	0.73

Table 2. Diffusion coefficient of V_2O_5 devices at various annealing temperatures.

and 300 °C were the lowest among all, measuring 6% and 3.25%, respectively. Owing to this extremely low optical contrast, no noticeable color change was observed. This phenomenon was attributed to the high surface roughness and large grain size of the thin films developed at higher annealing temperatures, which impeded Li^+ ion diffusion[53]. Similar findings have been reported by other researchers[7,53].

Table 4 summarizes the coloring and bleaching time (t_c, t_b), optical density (ΔOD), intercalated charges (Q_{in}), and coloration efficiency (CE) of V_2O_5 devices. Notably, an ideal EC device should demonstrate characteristics including rapid coloring and bleaching times, high optical density, minimal Q_{in}, as well as high CE. In this study, the V_2O_5 device annealed at 200 °C exhibited fast switching times, with coloring and bleaching times of 0.4 s and 3 s, respectively. The coloring time was determined by measuring the duration it takes for the device to change from its initial transparent state to 90% of the final optical state, while the bleaching time was defined as the time required for the device to return from its colored state to 90% of its original transparent state[58]. Furthermore, the results demonstrated that the bleaching time of all V_2O_5 devices was longer than the coloring time, potentially due to the uneven surfaces of V_2O_5 thin films, which caused inefficiencies in ion removal. This observation was consistent with the previous findings wherein the bleaching time of V_2O_5 thin films (2 s) could exceed the coloring time (1.6 s)[59]. Remarkably, V_2O_5 devices at all annealing temperatures demonstrated a rapid coloring time of less than 5 s, highlighting a fast ion diffusion process.

Coloration efficiency (CE) is defined as the ratio of optical density (ΔOD) to the intercalated charge per unit area, represented by the following equation[60]:

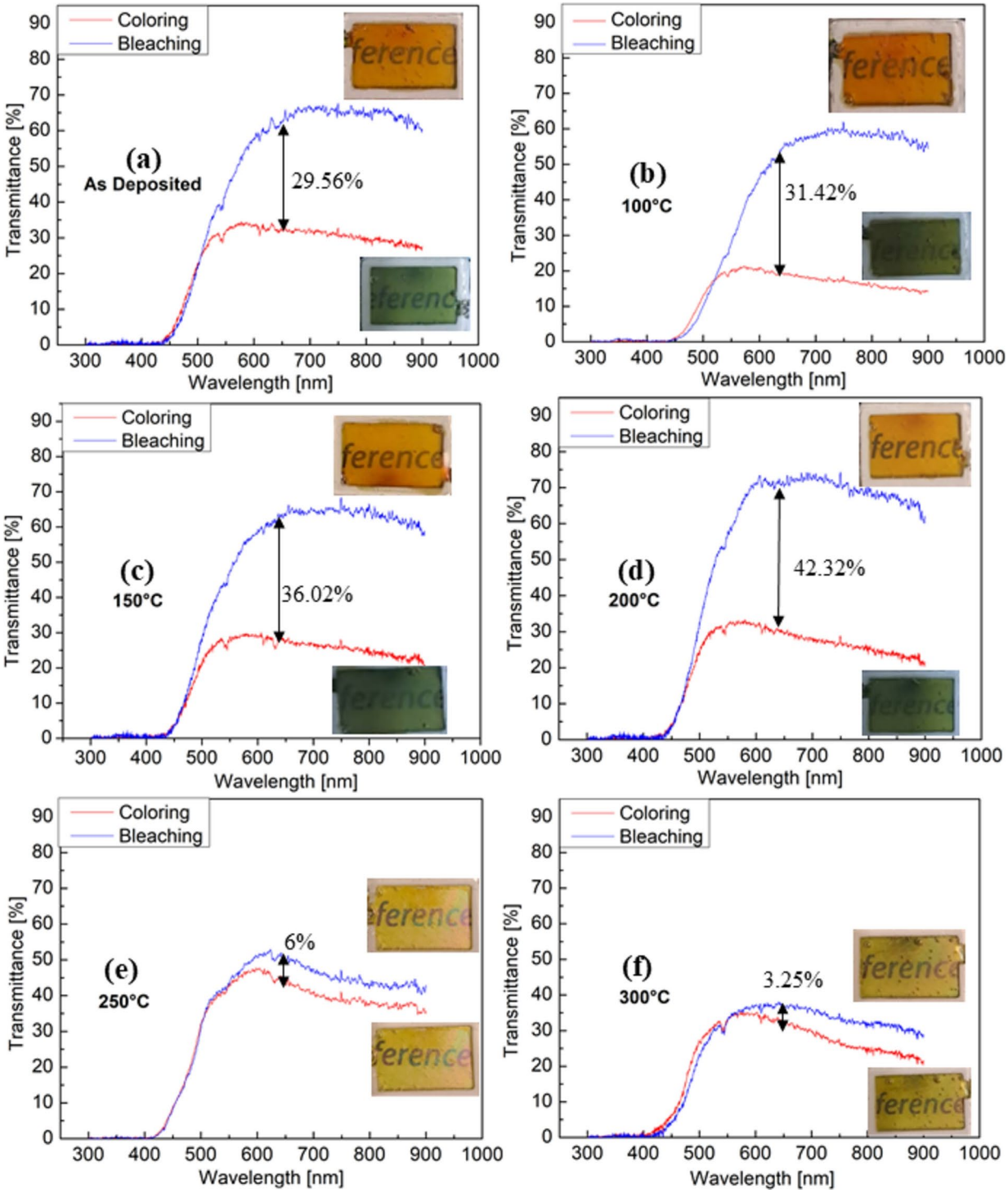

Fig. 8. Optical transmittances of V_2O_5 devices at (**a**) As Deposited (**b**) 100 °C (**c**) 150 °C (**d**) 200 °C (**e**) 250 °C (**f**) 300 °C.

$$CE = \frac{\Delta\,(OD)}{Q_{in}} = \frac{log\left(\frac{T_b}{T_c}\right)}{Q_{in}} \tag{4}$$

where T_b is the bleaching transmittance, T_c is the coloring transmittance, and Q_{in} is the intercalated charge per unit area. Table 4 reveals that the V_2O_5 device annealed at 200 °C exhibits the highest CE value of 34.93 cm^2/C, reflecting its excellent EC performance. Conversely, the V_2O_5 device annealed at 300 °C demonstrated the lowest CE value of 7.8 cm^2/C, attributable to its low optical modulation.

Temperature (°C)	Coloring Transmittance, T_c (%)	Bleaching Transmittance, T_b (%)	Optical Modulation, ΔT (%)
As Deposited	33.65	63.21	29.56
100	19.08	50.50	31.42
150	26.35	62.37	36.02
200	29.57	71.89	42.31
250	44.00	50.00	6.00
300	32.77	36.46	3.68

Table 3. Coloring and bleaching transmittances of V_2O_5 devices at various annealing temperatures.

Temperature (°C)	Coloring Time, t_c (s)	Bleaching Time, t_b (s)	Optical Density, ΔOD	Intercalated Charges, Q_{in} (C cm^{-2})	Coloration Efficiency, CE (cm^2 C^{-1})
As Deposited	0.5	5.12	0.27	− 0.010	27.16
100	0.6	5.42	0.42	− 0.013	30.95
150	0.5	4.42	0.37	− 0.012	31.69
200	0.4	3.00	0.38	− 0.011	34.93
250	0.6	2.32	0.055	− 0.003	15.69
300	0.8	4.12	0.046	− 0.006	7.80

Table 4. Coloring and bleaching kinetics of V_2O_5 devices at various post-annealing temperatures.

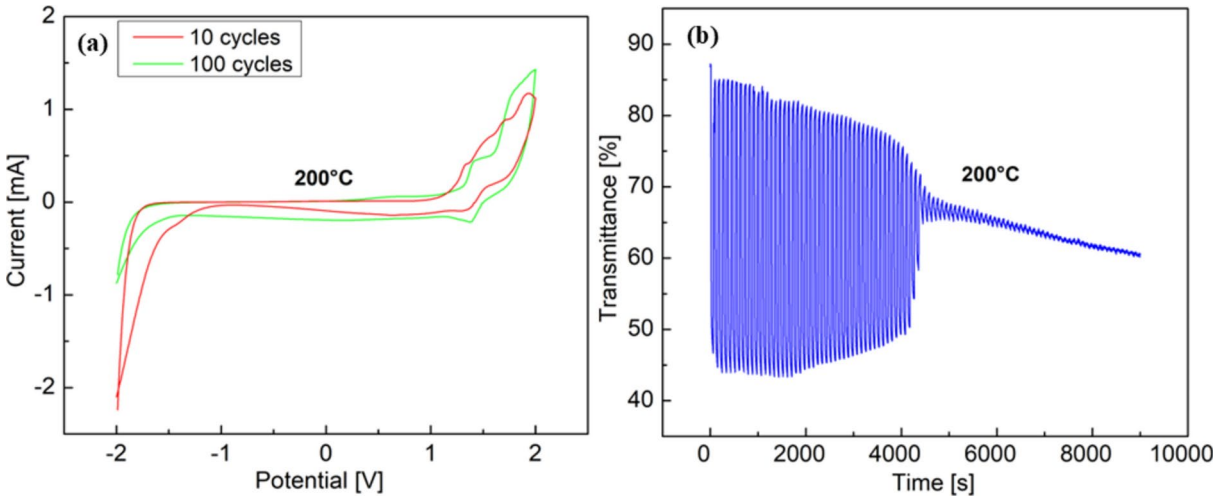

Fig. 9. (**a**) Cyclic voltammetry and (**b**) transmittance spectra of V_2O_5 devices annealed at 200 °C over 100 cycles.

Furthermore, the V_2O_5 device annealed at 200 °C underwent a cyclic stability assessment through continuous CV and CA measurements conducted over 100 cycles [see Fig. 9a and b]. Figure 9a demonstrates a decrease in the cathodic peak current from 2.24 to 1.78 mA after 100 cycles. Similarly, Fig. 9b illustrates a decline in optical contrast from 41 to 26% after 45 cycles, with complete degradation by the 100th cycle. Remarkably, the V_2O_5 device maintained acceptable optical contrast for 4500 s before significant degradation occurred. The low cyclic stability of V_2O_5 thin films was primarily attributed to morphological distortions that occurred during repeated ion intercalation and deintercalation. These structural changes caused ion trapping and incomplete ion diffusion within the V_2O_5 layers, leading to performance degradation over time[61]. Additionally, one study reported that applying a wide voltage range of − 2 to + 2 V generated gas bubbles within the device, which further compromised its longevity[62]. To address these challenges, researchers proposed several strategies. For example, doping V_2O_5 with metals such as titanium (Ti), molybdenum (Mo), tungsten (W), or niobium (Nb) was shown to enhance structural stability and improve cycling performance[62–64]. Another effective approach involved coating the thin films with a protective inorganic solid electrolyte (Li_3PO_4) to minimize direct interaction with the electrolyte and mitigate degradation[61].

Table 5 provides a comparative analysis of the EC performance of V_2O_5 thin films and devices fabricated using various methods and annealed at their respective optimal temperatures. This study stood out for its low

Authors	Optimal Temperature (°C)	Fabrication Method	Thin film/device	Optical Modulation, ΔT (%)	Coloration Efficiency, CE (cm^2 C^{-1})	Cyclic Stability
Tutel et al.[65]	450	Ultrasonic spray deposition	Thin film	17	–	25
Lin et al.[41]	400	RF co-sputtering	Thin film	31	6.3	–
Vernardou et al.[66]	300	Hydrothermal synthesis	Thin film	40	–	500
Mouratis et al.[67]	250	Spray pyrolysis	Thin film	7	8.1	–
Mjejri et al.[68]	500	Doctor blade	Thin film	51	–	300
This work	200	Sol–gel spin coating	Device	42.32	34.93	100

Table 5. A comparison of EC parameters between the current study and others.

annealing temperature of 200 °C, which was significantly lower than the temperatures reported by Mejri et al. (500 °C) and Tutel et al. (450 °C), highlighting its energy-efficient processing approach. Moreover, unlike other studies that focus solely on thin films, this work successfully incorporated a complete device, presenting a practical and scalable solution for real-world EC applications. Besides, the fabricated device demonstrated an optical modulation of 42.32%, making it highly competitive and second only to Mejri et al. (51%), while outperforming Tutel et al. (17%) and Mouratis et al. (7%). Furthermore, the coloration efficiency of 34.93 cm^2 C^{-1} significantly surpassed the values reported by Lin et al. (6.3 cm^2 C^{-1}) and Mouratis et al. (8.1 cm^2 C^{-1}). While the cyclic stability of 100 cycles was lower than that of Mejri et al. (300 cycles) and Veranadou et al. (500 cycles), the balance achieved between low-temperature processing, high optical modulation, and excellent coloration efficiency positions this fabrication method as a promising approach for developing practical multicolor EC devices.

Conclusion

In conclusion, V_2O_5 thin films were successfully fabricated using sol–gel spin coating technique at different annealing temperatures (100–300 °C). Subsequently, the thin films were converted into devices to study their EC performance. The V_2O_5 thin films annealed at varying temperatures exhibited thicknesses ranging from 273 to 332 nm. XRD analysis also indicated that higher annealing temperatures could significantly improve the crystallinity of these V_2O_5 thin films. Meanwhile, the CV analysis demonstrated that the V_2O_5 device annealed at 200 °C achieved a maximum diffusivity of 12.15×10^{-11} cm^2/s, which decreased significantly at higher temperatures. Additionally, the V_2O_5 device annealed at 200 °C exhibited the highest optical modulation of 42.32% and CE of 34.93 cm^2/C, whereas the device annealed at 300 °C obtained the lowest optical modulation of 3.25% and CE of 7.80%. Throughout this study, the V_2O_5 device annealed at 200 °C demonstrated the best EC performance with good diffusivity, high optical modulation of 42.32%, excellent CE of 34.93 cm^2/C, as well as rapid coloring (0.4 s) and bleaching time (3 s). This study showed a good correlation between the microstructure and EC performance of V_2O_5 devices under careful annealing control at low temperatures. These technical novelties also provide further increased awareness and research strategies for future modern electronic devices including multicolor EC windows, multicolor displays, and energy status indicators.

Data availability

All data generated or analysed during this study are included in this published article.

Received: 19 September 2024; Accepted: 30 December 2024
Published online: 07 January 2025

References

1. Shen, M., Huang, W., Chen, M., Song, B., Zeng, G. & Zhang, Y. (Micro)plastic crisis: Un-ignorable contribution to global greenhouse gas emissions and climate change. https://doi.org/10.1016/j.jclepro.2020.120138 (2020).
2. Yoro, K. O. & Daramola, M. O. CO_2 emission sources, greenhouse gases, and the global warming effect. In *Advances in Carbon Capture: Methods, Technologies and Applications*. https://doi.org/10.1016/B978-0-12-819657-1.00001-3 (2020).
3. Géczi, G., Benécs, J., Kristóf, K. & Horváth, M. High concentrations of radon and carbon dioxide in energy-efficient family houses without heat recovery ventilation. *J. Environ. Eng. Landsc. Manag.* https://doi.org/10.3846/16486897.2017.1347095 (2018).
4. Cannavale, A., Ayr, U., Fiorito, F. & Martellotta, F. Smart electrochromic windows to enhance building energy efficiency and visual comfort. *Energies (Basel)* https://doi.org/10.3390/en13061449 (2020).
5. Lv, Z., Yang, D., Mo, J., Jin, Z. & Chang, S. Construction of TiO_2/WO_3/TiO_2 double heterojunction films for excellent electrochromic performance. *Sci. Rep.* **14**(1), 11443. https://doi.org/10.1038/s41598-024-61911-9 (2024).
6. Piernas Muñoz, M. J. & Castillo Martínez, E. Prussian blue and its analogues. Structure, characterization and applications. In *SpringerBriefs in Applied Sciences and Technology*. https://doi.org/10.1007/978-3-319-91488-6_2 (2018).
7. Tan, M. Y. et al. Rapid post-annealing effect on the TiO_2-based electrochromic films. *Opt. Mater. (Amst.)* https://doi.org/10.1016/j.optmat.2023.114455 (2023).
8. Purushothaman, K. K., Muralidharan, G. & Vijayakumar, S. Sol-Gel coated WO_3 thin films based complementary electrochromic smart windows. *Mater. Lett.* https://doi.org/10.1016/j.matlet.2021.129881 (2021).
9. Bulja, S., Kopf, R., Tate, A. & Hu, T. High frequency dielectric characteristics of electrochromic, WO_3 and NiO films with $LiNbO_3$ electrolyte. *Sci. Rep.* https://doi.org/10.1038/srep28839 (2016).
10. Zhao, W. et al. Macroporous vanadium oxide ion storage films enable fast switching speed and high cycling stability of electrochromic devices. *ACS Appl. Mater. Interfaces* https://doi.org/10.1021/acsami.2c05492 (2022).
11. Zhao, L. et al. Constructed TiO_2/WO_3 heterojunction with strengthened nano-trees structure for highly stable electrochromic energy storage device. *J. Adv. Ceram.* https://doi.org/10.26599/JAC.2023.9220711 (2023).

12. Abe, Y., Kadowaki, Y., Kawamura, M., Kim, K. H. & Kiba, T. Two-color electrochromic devices using a tungsten oxide and nickel oxide double layer. *Jpn. J. Appl. Phys.* https://doi.org/10.35848/1347-4065/aca4b1 (2023).
13. Ko, T. F. et al. High-performance complementary electrochromic device based on iridium oxide as a counter electrode. *Materials* https://doi.org/10.3390/ma14071591 (2021).
14. Wen-Cheun Au, B., Tamang, A., Knipp, D. & Chan, K. Y. Post-annealing effect on the electrochromic properties of WO_3 films. *Opt. Mater. (Amst.)* https://doi.org/10.1016/j.optmat.2020.110426 (2020).
15. Thongpan, W. et al. Porous $CuWO_4/WO_3$ composite films with improved electrochromic properties prepared by sparking method. *Mater. Lett.* https://doi.org/10.1016/j.matlet.2019.126747 (2019).
16. Romanitan, C. et al. Structural investigations in electrochromic vanadium pentoxide thin films. *Phys. Status Solidi (a)* **219**(16), 2100431. https://doi.org/10.1002/PSSA.202100431 (2022).
17. Cestarolli, D. T., Guerra, E. M., Cestarolli, D. T. & Guerra, E. M. Vanadium pentoxide (V_2O_5): Their obtaining methods and wide applications. In *Transition Metal Compounds—Synthesis, Properties, and Application*. https://doi.org/10.5772/INTECHOPEN.96860 (2021).
18. Ashery, M. H., Elnouby, M., EL-Maghraby, E. M. & Elsehly, E. M. Structural control of V_2O_5 nanoparticles via a thermal decomposition method for prospective photocatalytic applications. *Beni Suef Univ. J. Basic Appl. Sci.* https://doi.org/10.1186/s43088-023-00350-3 (2023).
19. Fu, Q., Zhao, H., Sarapulova, A. & Dsoke, S. V_2O_5 as a versatile electrode material for postlithium energy storage systems. *Appl. Res.* **2**(3), e202200070. https://doi.org/10.1002/APPL.202200070 (2023).
20. Terán-Escobar, G., Pampel, J., Caicedo, J. M. & Lira-Cantú, M. Low-temperature, solution-processed, layered V_2O_5 hydrate as the hole-transport layer for stable organic solar cells. *Energy Environ. Sci.* **6**(10), 3088–3098. https://doi.org/10.1039/C3EE42204F (2013).
21. Schneider, K., Lubecka, M. & Czapla, A. V_2O_5 thin films for gas sensor applications. *Sens. Actuators B Chem.* https://doi.org/10.1016/j.snb.2016.04.059 (2016).
22. Hassan, B. F., Dathan, M. J. & Abdallah, A. A. Effects of annealing on the structural and optical properties of v2o5 thin films prepared by rf sputtering for humidity sensor application. *Iraqi J. Sci.* https://doi.org/10.24996/ijs.2021.62.10.12 (2021).
23. Verona, C. et al. Stability of H-terminated diamond MOSFETs with V_2O_5/Al_2O_3 as gate insulator. *IEEE Electron Device Lett.* https://doi.org/10.1109/LED.2019.2903578 (2019).
24. Le, T. K. *et al.* Recent advances in vanadium pentoxide (V2O5) towards related applications in chromogenics and beyond: fundamentals, progress, and perspectives. https://doi.org/10.1039/d1tc04872d (2022).
25. Shchegolkov, A. V., Tugolukov, E. N. & Shchegolkov, A. V. Overview of electrochromic materials and devices: Scope and development prospects. *Adv. Mater. Technol* **2**(18), 066–073. https://doi.org/10.17277/AMT.2020.02.PP.066-073 (2020).
26. Partlow, D. P., Gurkovich, S. R., Radford, K. C. & Denes, L. J. Switchable vanadium oxide films by a sol-gel process. *J. Appl. Phys.* https://doi.org/10.1063/1.350272 (1991).
27. Mousavi, M., Kompany, A., Shahtahmasebi, N. & Bagheri-Mohagheghi, M. M. Characterization and electrochromic properties of vanadium oxide thin films prepared via spray pyrolysis. *Mod. Phys. Lett. B* https://doi.org/10.1142/S0217984913501522 (2013).
28. Livage, J. Hydrothermal synthesis of nanostructured vanadium oxides. *Materials* https://doi.org/10.3390/ma3084175 (2010).
29. Arya, N., Verma, D. & Balakrishnan, V. Fabrication of vertically aligned CNT- vanadium oxide hybrid architecture with enhanced compressibility and supercapacitor performance. *Nanotechnology* https://doi.org/10.1088/1361-6528/aca619 (2023).
30. Kamaruddin, S. A. et al. Zinc oxide films prepared by sol-gel spin coating technique. *Appl. Phys. A Mater. Sci. Process.* https://doi.org/10.1007/s00339-010-6121-2 (2011).
31. Aslan, N., Topuz, M., Aksakal, B. & Dikici, B. Production technique–structure relationship in bioceramic-coated scaffold applications. *Adv. Ceram. Coat. Biomed. Appl.* https://doi.org/10.1016/B978-0-323-99626-6.00005-6 (2023).
32. Incecam, S., Saraç, A., Erdil, E., Çğrtekin, A. & Acar, A. Effect of post-annealing treatment on the structural, optical, and electrical properties of V_2O_5 thin films. In *Gazi University Journal of Science Part A: Engineering and Innovation*, vol. 8, pp. 299–307 (2021).
33. Toe, M. Z., Matsuda, A., Han, S. S., Yaacob, K. A. & Pung, S. Y. Effect of annealing temperature on the performance of zno thin film-based dye sensitized solar cell. *AIP Conf. Proc.* https://doi.org/10.1063/5.0015699 (2020).
34. Yan, J., Zhou, T., Masuda, J. & Kuriyagawa, T. Modeling high-temperature glass molding process by coupling heat transfer and viscous deformation analysis. *Precis. Eng.* https://doi.org/10.1016/j.precisioneng.2008.05.005 (2009).
35. Bae, J. et al. Optimized low-temperature fabrication of WO_3 films for electrochromic devices. *J. Phys. D Appl. Phys.* https://doi.org/10.1088/1361-6463/aa8e88 (2017).
36. Dalavi, D. S., Bhosale, A. K., Desai, R. S. & Patil, P. S. Energy efficient electrochromic smart windows based on highly stable CeO_2-V_2O_5 optically passive counter electrode. *Mater. Today Proc.* https://doi.org/10.1016/j.matpr.2020.06.146 (2020).
37. Chan, K. Y., Au, B. W. C., Sahdan, M. Z., Chong, A. S. I. & Knipp, D. Realisation of solid-state electrochromic devices based on gel electrolyte. *F1000Res* https://doi.org/10.12688/f1000research.73661.2 (2022).
38. Thakur, V. K., Ding, G., Ma, J., Lee, P. S. & Lu, X. Hybrid materials and polymer electrolytes for electrochromic device applications. *Adv. Mater.* https://doi.org/10.1002/adma.201200213 (2012).
39. Baba, M. A., Gasim, A., Awadelgied, A. M., Almuslet, N. A. & Salih, A. M. Influence of the annealing temperature on the thickness and roughness of $La_2Ti_2O_7$ thin films. *Adv. Mater. Phys. Chem.* https://doi.org/10.4236/ampc.2020.108014 (2020).
40. Kabir, M. H., Ali, M. M., Kaiyum, M. A. & Rahman, M. S. Effect of annealing temperature on structural morphological and optical properties of spray pyrolized Al-doped ZnO thin films. *J. Phys. Commun.* https://doi.org/10.1088/2399-6528/ab496f (2019).
41. Lin, T. C., Jheng, B. J., Yen, H. M. & Huang, W. C. Thermal annealing effects of V_2O_5 thin film as an ionic storage layer for electrochromic application. *Materials* https://doi.org/10.3390/ma15134598 (2022).
42. Yelsani, V., Pothukanuri, N., Sontu, U. B., Yaragani, V. & Musku Venkata, R. R. Effect of annealing temperature on structural, morphological, optical and electrical properties of spray deposited V_2O_5 thin films. *Mater. Sci.* https://doi.org/10.5755/j01.ms.25.1.22435 (2019).
43. Mohsin Mahdi, S. Morphological and optical properties of V_2O_5:TiO_2 thin film prepared by PLD technique. *Iraqi J. Phys.* https://doi.org/10.30723/ijp.v17i43.464 (2019).
44. Gandasiri, R., Sreelatha, C. J., Nagaraju, P. & Vijayakumar, Y. Effect of annealing temperature on micro-structural, optical and electrical characterization of nanostructured V_2O_5 thin films prepared by spray pyrolysis technique. *Phys. B Condens. Matter.* https://doi.org/10.1016/j.physb.2019.08.004 (2019).
45. Yelsani, V., Pothukanuri, N., Sontu, U. B., Yaragani, V. & Musku Venkata, R. R. Effect of annealing temperature on structural, morphological, optical and electrical properties of spray deposited V_2O_5 thin films. *Medziagotyra* https://doi.org/10.5755/j01.ms.25.1.18492 (2019).
46. Cardozo Amorin, L. H., Da Silva Martins, L., Lopes, F. & Urbano, A. Thickness effect on the optical band gap of V_2O_5 thin films deposited by thermal evaporation. *Semina: Ciências Exatas e Tecnológicas* https://doi.org/10.5433/1679-0375.2017v38n2p59 (2018).
47. Zaier, A., Meftah, A., Jaber, A. Y., Abdelaziz, A. A. & Aida, M. S. Annealing effects on the structural, electrical and optical properties of ZnO thin films prepared by thermal evaporation technique. *J. King Saud Univ. Sci.* https://doi.org/10.1016/j.jksus.2015.04.007 (2015).
48. Zhang, G. et al. Effects of annealing temperature on optical band gap of sol-gel tungsten trioxide films. *Micromachines (Basel)* https://doi.org/10.3390/mi9080377 (2018).

49. Venkatachalapathy, R., Haris, M. & Murugesan, R. Structural, Morphological, Optical, Luminescent and Magnetic Properties of Nanostructured ZnO Thin Film. https://doi.org/10.21203/rs.3.rs-243700/v1 (2021).
50. Zimmer, A., Tresse, M., Stein, N., Horwat, D. & Boulanger, C. Towards enhanced durability of electrochromic WO_3 interfaced with liquid or ceramic sodium-based electrolytes. *Electrochim. Acta* https://doi.org/10.1016/j.electacta.2020.136931 (2020).
51. Özdemir, O. et al. Nano-crystal $V_2O_5nH_2O$ sol-gel films made by dip coating. *AIP Conf. Proc.* https://doi.org/10.1063/1.4751601 (2012).
52. Benmoussa, M., Outzourhit, A., Jourdani, R., Bennouna, A. & Ameziane, E. L. Structural, optical and electrochromic properties of sol-gel V_2O_5 thin films. *Act. Passiv. Electron. Compon.* https://doi.org/10.1080/0882751031000116223 (2003).
53. Verma, A., Basu, A., Bakhshi, A. K. & Agnihotry, S. A. Structural, optical and electrochemical properties of sol-gel derived TiO_2 films: annealing effects. *Solid State Ion* **176**(29–30), 2285–2295. https://doi.org/10.1016/j.ssi.2005.06.011 (2005).
54. Abareshi, A. & Haratizadeh, H. Effect of annealing temperature on optical and electrochromic properties of tungsten oxide thin films. *Iran. J. Phys. Res.* https://doi.org/10.18869/acadpub.ijpr.16.3.47 (2016).
55. Bai, L. et al. Direct electrochemistry and electrocatalysis of a glucose oxidase-functionalized bioconjugate as a trace label for ultrasensitive detection of thrombin. *Chem. Commun.* https://doi.org/10.1039/c2cc35295h (2012).
56. Wu, C. L., Lin, C. K., Wang, C. K., Wang, S. C. & Huang, J. L. Annealing induced structural evolution and electrochromic properties of nanostructured tungsten oxide films. *Thin Solid Films* https://doi.org/10.1016/j.tsf.2013.06.022 (2013).
57. Chen, X. et al. Annealing effect on the electrochromic properties of amorphous WO_3 films in Mg^{2+} based electrolytes. *Mater. Chem. Phys.* https://doi.org/10.1016/j.matchemphys.2021.124745 (2021).
58. Hassab, S. et al. A new standard method to calculate electrochromic switching time. *Sol. Energy Mater. Sol. Cells* https://doi.org/10.1016/j.solmat.2018.04.031 (2018).
59. Ma, X. et al. Synthesis and electrochromic characterization of graphene/V_2O_5/MoO_3 nanocomposite films. *ECS J. Solid State Sci. Technol.* https://doi.org/10.1149/2.0031610jss (2016).
60. More, A. J. et al. Electrodeposition of nano-granular tungsten oxide thin films for smart window application. *Mater. Lett.* https://doi.org/10.1016/j.matlet.2014.07.059 (2014).
61. Lee, S. H., Cheong, H. M., Liu, P. & Tracy, C. E. Improving the durability of amorphous vanadium oxide thin-film electrode in a liquid electrolyte. *Electrochem. Solid-State Lett.* https://doi.org/10.1149/1.1567533 (2003).
62. Shin, D. et al. Evaluation of low-voltage-driven multi-colored electrochromic device based on dry-deposited V_2O_5. *Sol. Energy Mater. Sol. Cells* https://doi.org/10.1016/j.solmat.2023.112341 (2023).
63. Westphal, T. M. et al. Influence of the Nb_2O_5 doping on the electrochemical properties of V_2O_5 thin films. *J. Electroanal. Chem.* https://doi.org/10.1016/j.jelechem.2017.02.014 (2017).
64. Wei, Y., Zhou, J., Zheng, J. & Xu, C. Improved stability of electrochromic devices using Ti-doped V_2O_5 film. *Electrochim. Acta* https://doi.org/10.1016/j.electacta.2015.03.087 (2015).
65. Tutel, Y. et al. Multichromic vanadium pentoxide thin films through ultrasonic spray deposition. *J. Electrochem. Soc.* https://doi.org/10.1149/1945-7111/ac2dcf (2021).
66. Vernardou, D., Louloudakis, D., Spanakis, E., Katsarakis, N. & Koudoumas, E. Electrochemical properties of vanadium oxide coatings grown by hydrothermal synthesis on FTO substrates. *New J. Chem.* https://doi.org/10.1039/c3nj00931a (2014).
67. Mouratis, K. *et al.* Electrochromic performance of V_2O_5 thin films grown by spray pyrolysis. https://doi.org/10.3390/ma13173859 (2020).
68. Mjejri, I., Rougier, A. & Gaudon, M. Low-cost and facile synthesis of the vanadium oxides V_2O_3, VO_2, and V_2O_5 and their magnetic, thermochromic and electrochromic properties. *Inorg. Chem.* https://doi.org/10.1021/acs.inorgchem.6b02880 (2017).

Acknowledgements

This work was funded by the Telekom Malaysia Research and Development (TM R&D) under TM R&D Research Fund (Grant No: RDTC/231080, Project ID: MMUE/230009).

Author contributions

Conceptualization, M. Y. T, K. Y. C.; methodology, M. Y. T., K. Y. C.; validation, K. Y. C., G. S. H. T., K. B. T., H. C. A. M.; formal analysis, M. Y. T., K. Y. C. ; investigation, M. Y. T., K. Y. C.; re-sources, K. Y. C; data curation, M. Y. T.; writing—original draft preparation, M. Y. T.; writing—review and editing, K. Y. C., K. B. T., H. C. A. M; visualization, G. S. H. T., K. B. T., H. C. A. M.; supervision, K. Y. C.; project administration, K. Y. C.; funding acquisition, K. Y. C. All authors have read and agreed to the published version of the manuscript.

Declarations

Competing interests

The authors declare no competing interests.

Additional information

Supplementary Information The online version contains supplementary material available at https://doi.org/10.1038/s41598-024-85014-7.

Correspondence and requests for materials should be addressed to K.-Y.C.